Carbon 200 (2022) 108–115

Contents lists available at ScienceDirect

Carbon

journal homepage: www.elsevier.com/locate/carbon

Mechanical behavior and micro-mechanism of carbon nanotube networks under friction

Tianxiong Hu [a,c], Guian Qian [a,c], Xianqian Wu [b,c], Chao Wang [a,c,*]

[a] LNM, Institute of Mechanics, Chinese Academy of Sciences, Beijing, 100190, China
[b] LMFS, Institute of Mechanics, Chinese Academy of Sciences, Beijing, 100190, China
[c] School of Engineering Science, University of Chinese Academy of Sciences, Beijing, 100049, China

ARTICLE INFO

Keywords:
Carbon nanotube network
Friction
Crosslink
Deformation behavior
Coarse-grained molecular dynamics

ABSTRACT

Friction behavior of carbon nanotube networks (CNNs) is ubiquitous in applications, however, is poorly investigated. Here, we employ coarse-grained molecular dynamics (CGMD) simulations to investigate friction behaviors and microscopic mechanism of CNNs. We first give a phase diagram to determine the initial contacting state of "supported" or "trapped" for an indenter in CNNs. In a "supported" state, friction force is mainly originated from the local surface adhesion of CNNs which experience stable elastic deformation in friction process. In contrast, in a "trapped" state, friction force is mainly activated by nonlocal reconstitution of carbon nanotubes (CNTs) accompanied with irreversible bond breaking. Furthermore, with an increased normal pressure, the friction force keeps nearly constant for a "supported" indenter while it increases linearly for a "trapped" one; the friction force is linearly or nonlinearly related to the sliding velocity of an indenter in a supported or trapped state. Importantly, there is a critical crosslink density, above which, the coefficient of friction is greatly decreased due to enhanced integrity of CNNs. These results provide a profound understanding of friction deformation behavior of CNNs, which is of great significance for optimal design in practical applications.

1. Introduction

Carbon nanotube network (CNN) materials are assembled by a large number of carbon nanotubes (CNTs) in a random or regular spatial distribution. They have drawn wide attention due to their light weight [1], remarkable mechanical [2], thermal [3] and electrical [4] properties. Both CNNs and their composites find wide potential applications in both traditional industrial fields, such as lightning strike protection system of vehicle and airplanes [5], and emerging fields of flexible devices [6], water treatment membranes [7] and medical implants [8].

Most researchers are dedicated to unveil the deformation and failure mechanisms to continuously improve mechanical performance of CNN materials under tension, compression and impaction conditions. Ma et al. [9] found that good and long inter-bundle connections as physical crosslinkers are responsible for the strength (up to 360 MPa) of single-walled CNN films. Li et al. [10] further found that the entanglement and bundling mechanisms affect major structural features of buckypaper by the coarse-grained molecular dynamics (CGMD) method. Chen et al. [11] and Jakubinek et al. [12] found that the strength of pristine CNNs can be increased by 1–4 times by adding chemical groups as crosslinkers to strengthen junctions of adjacent CNTs, which is further validated by Wang et al. [13] and Yang et al. [14] using the CGMD method. Xie et al. [15] and Wang et al. [16] found that crosslinkers can further improve strain affinity and avoid the pull-out failure of CNN materials. Wu et al. [17] and Wang et al. [18] found discrete and mobile nanoparticles strengthen inter-tube joints and constrain the bundling of CNTs to increase the Young's modulus and the tensile strength. Wang et al. [19] studied the dissipation of CNN materials under impaction and pointed out that the brittle fracture of carbon nanotubes and ductile fracture of van der Waals interfaces between the nanotubes in forms of detachments or sliding are the channels to dissipate mechanical energy. Later, Xiao et al. [20] studied the similar impaction behavior of CNN materials and observed a mode transition from bending-dominated dissipation to stretching-bending-dominated one by tuning the fraction of strong crosslinkers. Very recently, Yu et al. [21] found that double-crosslinked CNNs can nicely achieve cooperative energy dissipation with minimal structural damage by applying CGMD simulations. Xu et al. [22] made a CNN material composed of long interconnected CNTs and found an important temperature- and frequency-irrelevant viscoelastic properties under cyclic shear loadings. This important

* Corresponding author. LNM, Institute of Mechanics, Chinese Academy of Sciences, Beijing, 100190, China.
E-mail address: wangchao@lnm.imech.ac.cn (C. Wang).

https://doi.org/10.1016/j.carbon.2022.08.042
Received 23 May 2022; Received in revised form 30 July 2022; Accepted 10 August 2022
Available online 21 August 2022

viscoelastic property of CNN materials is further explained using the microscopic mechanisms of "zipping-unzipping" and unstable "attachments/detachments" between individual CNTs by Li et al. [23] and Yang et al. [24], respectively. Xu et al. [25] and Ma et al. [26] observed a changing Poisson's ratio from negative to positive through the reorientation of CNT bundles, which was explained by Rawal et al. [27] using a simple geometric model recently. Pan et al. [28] and Chen et al. [29] studied the stiffness threshold and found two critical network densities dividing the stiffness behavior into three stages: zero stiffness, bending dominated and stretching dominated stages.

Besides of the researches on pure CNN materials, the effect of length [30], reorientation [31], reconnection [32] of CNTs, and stability and porous structure [33] on mechanical properties of CNN-based composites are also investigated extensively to ensure industrial applications [34–37].

These studies pave a way to understand deformation behaviors of CNNs and related composites under tension, compression, impaction. However, in most practical applications, friction of both CNN materials and CNN-based composites are ubiquitous and play an important role in full play of different functions. For example, CNNs significantly reduce the abrasive wear between alloys in the automation, aerospace, and chemical industries [38]. However, friction of CNNs or related-composites is much different from that of metals [39,40] or various two-dimensional materials [41,42]. The surface of metals or two-dimensional materials are atomically dense and the friction is mainly induced by dislocation propagation and annihilation or lattice incommensurability. For the CNNs and related-composites with intrinsic porous and irregular microstructures at surfaces, the microscopic sags and crests on contacting objects would be pressed into porous structure of CNNs under normal pressure, which would cause complex friction and scratch behaviors of carbon nanotubes in sliding process. Some interesting phenomena have been observed: Fei et al. [43] found the coefficient of friction (COF) of carbon fiber reinforced material prepared with cashew-modified phenolic resin decreased with the increased normal pressure, which is much different from the pressure-independent COF for most conventional materials [44,45]. The underlying mechanisms could not be explained using the reported micro-mechanisms in above references and remain poorly understood up to now.

Here, we adopt a CGMD method to study the relationship between porous network structures and friction properties of CNN materials, including contacting state, normal pressure, sliding speed and crosslink density. This paper is organized as below. The mesoscopic numerical model of CNNs is first given in the second part. In the third part, two normalized quantities of indenter size and normal pressure are proposed to characterize two typical contacting states of "supported" and "trapped" for an indenter on CNNs. Then, the friction mechanism of an indenter in the two contacting states are meticulously studied. Furthermore, the effect of normal pressure, sliding velocity and crosslink density of CNNs on friction behaviors are analyzed in the fourth part. A conclusion is given at last.

2. Numerical model and methodology

A well-validated coarse-grained bead-spring model of CNT proposed by Buehler [46] is used to establish the numerical model of CNNs. The energy of a single CNT is characterized by the tensile energy $E_T = k_T (r\text{-}r_0)^2/2$ of all bonds in the CNT, the bending energy $E_\theta = k_\theta (1+\cos\theta)$ of all triplets in the CNT and the van der Waals energy $E_{pairs} = 4\varepsilon[(d_{zero\text{-}energy}/d)^{12}\text{-}(d_{zero\text{-}energy}/d)^6]$ with other neighbor CNTs, where k_T, k_θ, θ, r, r_0 are the tensile stiffness, bending stiffness, the angle of the triplet, current bond length and the equilibrium one, respectively. ε, d and $d_{zero\text{-}energy}$ denote the energy well depth, the distance between the beads in neighbor CNTs, and the zero-energy distance, respectively. The parameters of main force field used in this paper are listed in Table 1, which is calibrated from full-atom MD simulation, see the original work [46,47] for more details. The bond would break as its tensile strain exceeds a critical value 0.2 according to the experimental measurement of fracture strain of CNTs [2]. The mass for each coarse bead is 1953.23 amu (atomic mass unit). More details about the coarse-grained scheme of carbon nanotubes can be found in Refs. [47,48].

Table 1
The parameters for a (5,5) carbon nanotube in the CGMD [47].

Parameters	Values
Equilibrium inter-bond distance r_0 (Å)	10
Tensile stiffness k_T (kcal mol^{-1} Å^{-2})	1000
Equilibrium angle α_0 (°)	180
Bending stiffness k_θ (kcal/mol)	14300
Lennard-Jones parameter ε (kcal/mol)	15.1
Lennard-Jones parameter $d_{zero\text{-}energy}$ (Å)	9.35

Fig. 1a shows the numerical model of a CNN film with the microstructure of randomly-distributed CNTs (blue lines) entangled with each other (see a randomly-chosen entanglement point in Fig. 1a–II) and strengthened by crosslinks (see the magnified red bar in Fig. 1a–III) between neighbor CNTs. This numerical model is established by randomly generating 100 carbon nanotubes with the contour length of 100 nm in a simulation box. The two 100 is chosen by considering both the computational efficiency and the reasonability of the numerical model of CNN films. These nanotubes are first deposited layer by layer on a rigid substrate at the bottom of the simulation box to form a loose CNN sample under the action of a force pointing to the substrate (mimic the action of gravity). A Langevin thermostat with 300K and a Berendsen barostat with 0 Pa are taken in the isothermal-isobaric ensemble (NPT) [49]. Periodic boundary conditions are added both in x and y directions, but a free one in z direction. So, a thin CNN film with finite thickness and infinite length and width is obtained. When the total energy fluctuation is less than 0.1%, the model is considered to be in equilibrium. Then the substrate and the action force are removed, and a pure CNN film is obtained. After that, a detection program is adopted to find out all adjacent beads within 0.9–1.1 nm and belonging to different CNTs, a range around the equilibrium length of 1 nm for bonds in CNTs. Some pairs are then chosen randomly to generate crosslinks between the two beads in the pair according to the crosslink density (the effect is given in Fig. 7) as shown in Fig. 1a–III. This process is corresponding to the experiments [50,51], in which a strongly crosslinked CNN film is always made through two steps: a pure CNN film is first synthesized and then the strongly chemical and/or physical crosslinks are added between adjacent carbon nanotubes. The newly obtained numerical crosslinked CNN samples are exerted successively the geometrical optimization and the dynamic energy optimization at a Langevin thermostat with 300K and a Berendsen barostat with 0 Pa in both x and y directions to obtain a well-equilibrated system with a convergent total energy as shown in Fig. 1b. The whole film reaches a nearly zero-stress state marked by the stress component σ_{xx} as shown in the inset of Fig. 1b. The density of the obtained CNN film is 0.28 g/cm^3, which is comparable to the CNT network materials fabricated in the experiment [52]. Details of the numerical fabrication of a crosslink strengthened CNN film are referred to our previous works [13,14,18,53,54] about the tensile and compressive properties of CNNs.

Then, the configuration of the friction model is schematically shown in Fig. 1c, a piece of well-equilibrated CNN film with the length of 120 nm, the width of 70 nm and the height of 10 nm is put on a virtual rigid substrate as it is pressed and scratched by an indenter. In order to simplify the model and save computing time, we do not use any specific material to simulate the substrate, but just apply an action to the CNNs as the beads of CNNs is pressed into the upper boundary of the virtual substrate. This function is realized using the command of "fix wall/lj126" in LAMMPS, see more details in the manual of this command which can be easily accessed in the internet. The action potential energy is described using $E_{sp} = 4\varepsilon_{sp}[(d_{sp}/d)^{12}\text{-}(d_{sp}/d)^6]$, where d is the distance from the bead to the upper boundary of the substrate; ε_{sp} and d_{sp} are the

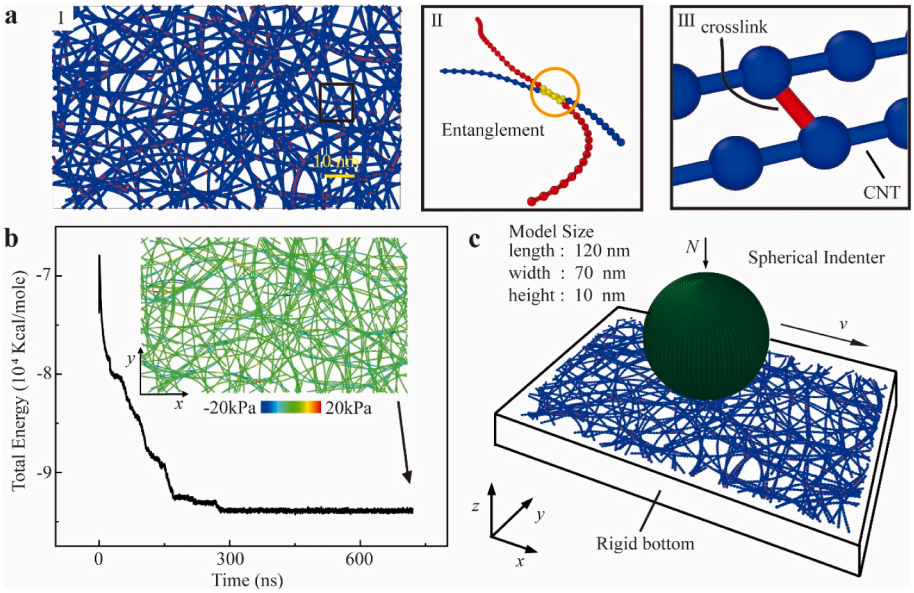

Fig. 1. The numerical model of CNNs and settings of the friction system. (a) The numerical sample of CNNs (blue) with entanglements points (color-coded by yellow in a-II) and crosslinks (red bar in a-III) between neighbor CNTs; Scale bar, 10 nm; (b) The total energy with relaxing time to obtain a well-equilibrated CNN film sample. Inset: the resulting equilibrated structure color-coded by the stress component σ_{xx}. (c) Schematic diagram of friction model and parameter settings. (A colour version of this figure can be viewed online.)

usual Lennard-Jones parameters denoting the energy well depth and the zero-energy distance, respectively. After the calculation as given in Fig. S1 in Supplementary Materials, a finite value for ε_{sp} is OK to reach the supporting effect. For simplicity, $\varepsilon_{sp} = \varepsilon$ and $d_{sp} = d_{\text{zero-energy}}$ are set in this paper, where ε and $d_{\text{zero-energy}}$ are given above. A rigid spherical indenter is put on the top of the CNNs and can slide on the film along x-direction under a downward normal force N in z-direction. The spherical rigid indenter is composed of beads as shown in Fig. 1c. The interaction between the beads in the indenter and the beads in CNN film is described using $E_{ip} = 4\varepsilon_{ip}[(d_{ip}/d)^{12}\text{-}(d_{ip}/d)^{6}]$, where d is the distance between the bead in the indenter and the bead in CNN, ε_{ip} and d_{ip} are the usual Lennard-Jones parameters denoting the corresponding energy well depth and the zero-energy distance, respectively. Like the settings of ε_{sp} and d_{sp}, we set $\varepsilon_{ip} = \varepsilon$ and $d_{ip} = d_{\text{zero-energy}}$ in all our simulations for simplicity.

In all our simulations, the periodic boundary conditions are adopted in both x and y directions and a free one in z direction. The Langevin thermostat with 300K and the Berendsen barostat with 0 Pa in both x and y directions are taken. The time step is 1 fs (1 fs = 10^{-15}s). All simulations are based on the large-scale atomic/molecular massively parallel simulator (LAMMPS) [55]. And the results are visualized based on Open Visualization Tool (OVITO) [56].

3. Results and discussions

3.1. Two typical contacting states of a spherical indenter on a CNN film

Before studying the dynamic friction behavior of an indenter on a CNN film, we first study the static contacting behavior of an indenter on a CNN film under a normal pressure by conducting systematic simulations. We examine the effect of two dimensionless quantities of normalized indenter size R and normalized pressure σ on the static contacting behavior of an indenter on a porous CNN film. R and σ are defined as $R = R_{\text{indenter}}/R_{\text{cnn}}$ and $\sigma = \sigma_n/\sigma_{\text{cnn}}$, where R_{indenter} is the radius of the indenter, R_{cnn} is the average pore radius of the film ~3.2 nm. See the calculation method of the radius of pores in Fig. S2 in Supplementary Materials. σ_n is the normal pressure calculated by $\sigma_n = N/S$, where N is the normal force and S is the effective contact area of the compression zone. The calculation method of the effective contact area of the compression zone is described in detail in Supplementary Materials. $\sigma_{\text{cnn}} = 250$ MPa is the in-plane tensile strength of CNNs obtained in our previous work [14] studying the large-deformation behaviors and fracture mode of CNN materials.

As shown in Fig. 2, by conducting systematic simulations with varied combination of σ and R represented by solid/hollow points, we obtain a critical line color-coded in red which divides the σ -R plane into two parts representing the two contacting states of "supported" and "trapped" for an indenter on a CNN film. In the "supported" state, the indenter slightly contacts with the film, while in the "trapped" state, the indenter is heavily pressed into the film and almost half of the lower part of the indenter is immersed in the film as illustrated by the two insets in Fig. 2. According to our simulations, the indentation depth in the "supported" state is about 0.05R which is larger than that in the friction of metals [39,40] or various two-dimensional materials [41,42]. For a given indenter with a normalized indenter size R, there exists a critical normal pressure σ_c at which the contacting state of the indenter changes

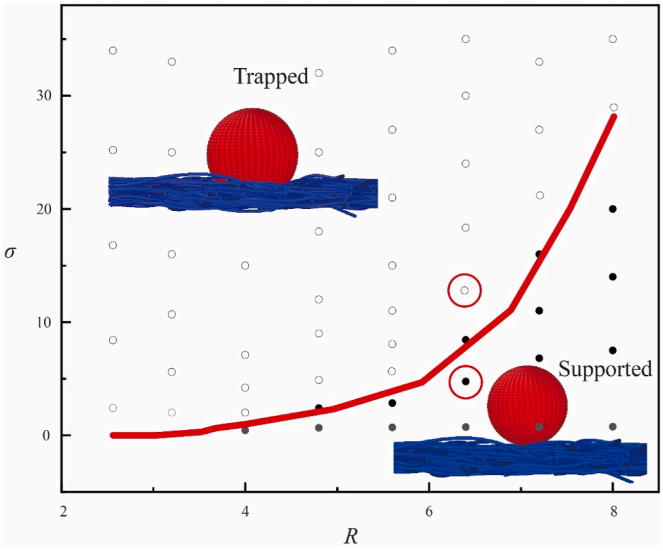

Fig. 2. The contacting state of a spherical indenter on a CNN film. The red thick line divides the σ-R plane into two parts: the top part filled with white hollow points is the "trapped" state of the indenter and the down part filled with solid black points is the "supported" one. All points are obtained by conducting a series of CGMD simulations. Two insets: the schematic of the two contacting states of the indenter. Two points highlighted by red circles are chosen for the following analysis. (A colour version of this figure can be viewed online.)

from "supported" to "trapped". And for a given normal pressure, it is reasonable that the larger an indenter is, the harder to push it into a porous material. Yosuke et al. [57] experimentally studied the wear properties of carbon nanotube films attached to copper based on an atomic force microscope (AFM), and observed the similar transition of contacting states and the contact-dependent wear behaviors as the normal load is increased. This indenter size-dependency is the main characteristic of the contacting and friction behavior of porous CNN materials, which is much different from that of non-porous materials of metals [39] and two-dimensional materials [41,42]. It should be noted that the basic relation between the normalized indenter size and normalized pressure shown in Fig. 2 also holds for the contact behavior of microscale or larger indenters. Having the two typical states of an indenter on a porous CNNs at hand, we are now in a position to study friction behaviors of an indenter in the two states.

3.2. Friction behavior of an indenter in a "supported" state

In order to study the friction behavior of an indenter in a "supported" state, we randomly choose a combination of the two key factors of $R = 6.3$ and $\sigma = 3.3$ which is under the red boundary line on the σ-R phase diagram as circled in Fig. 2. The sliding velocity of the indenter is set to be 10 m/s and the effect of the sliding velocity is studied later in Section 3.5. Fig. 3a shows the top view of a CNN film before friction sliding and the initial position of an indenter signed by a black cross on the film. The CNN film in the initial state is well equilibrated as color-coded by the value of σ_{xx}. Here, we noted that, because the indenter slides along the x direction (the friction direction), relatively speaking, more CNTs have larger σ_{xx} component as seen in the stress distribution diagram at an intermediate moment during friction process in Fig. S3 in Supplementary Material. So, we just give the stress component σ_{xx} in the text to demonstrate the basic characteristic of stress distribution. Fig. 3b shows the final state of the CNN film after the friction of the indenter. Comparing the configurations of the CNN film in the two states, it is clearly shown that both the topology and the stress state of the CNN film change negligibly in friction process. This is due to the slight elastic contact between the CNN film and the indenter in the "supported" state, CNT fibers deform elastically as they touch with the indenter and recover almost completely after the indenter sliding away from them.

To study the dependency of dynamic friction force f normalized by $\sigma_{cnn}S$ on surface topology, we measure the relative height of the region ahead of the sliding indenter as well as the dynamic friction force at the corresponding time, see the details of the calculation of the dynamic friction force in Supplementary Material. As shown in Fig. 3c–I, due to the intrinsic uneven porous surface structure, the height of the region ahead of the sliding indenter varies constantly in the sliding process of the indenter and the maximal variation of height is ~20 nm comparable to the size of the indenter. Here, we call the unevenness of the height of CNN surface to be roughness. The roughness of the CNN film can be divided into two kinds: the smaller roughness induced by the local randomly stacked CNTs as illustrated by the lower inset in Fig. 3c–I, and the larger structural humps as demonstrated schematically by the upper inset in Fig. 3c–I. The dynamic friction force also fluctuates greatly in the friction process of the indenter, with the maximal variation surpassing 980% as shown in Fig. 3c–II.

More interestingly, the fluctuation of the height ahead of the sliding indenter (see the details of the calculation of the height ahead of the sliding indenter in Fig. S4 in Supplementary Material) is well consistent with that of the dynamic friction force as indicated by the dotted red lines connecting Fig. 3c–I and II at several typical sliding positions. That is, a larger friction resistance would be triggered as higher humps appear in front of the sliding indenter. It is noted that the entanglement number of the CNN film is almost unchanged as the red solid line shown in Fig. 3c–I because of the negligible change of the topology of CNN film during the friction process of the indenter as shown in Fig. 3a and b.

It could be seen that the smaller friction force is mainly triggered by the smaller roughness induced by the local randomly stacked CNTs contacting with the indenter, while the larger one is triggered by the larger hump structures contacting with the indenter. It is noted that no matter the friction force is larger or smaller, it is mainly originated from local elastic interactions between the surrounding CNTs and the indenter, which is much different from the following friction behavior of the indenter in a "trapped" state.

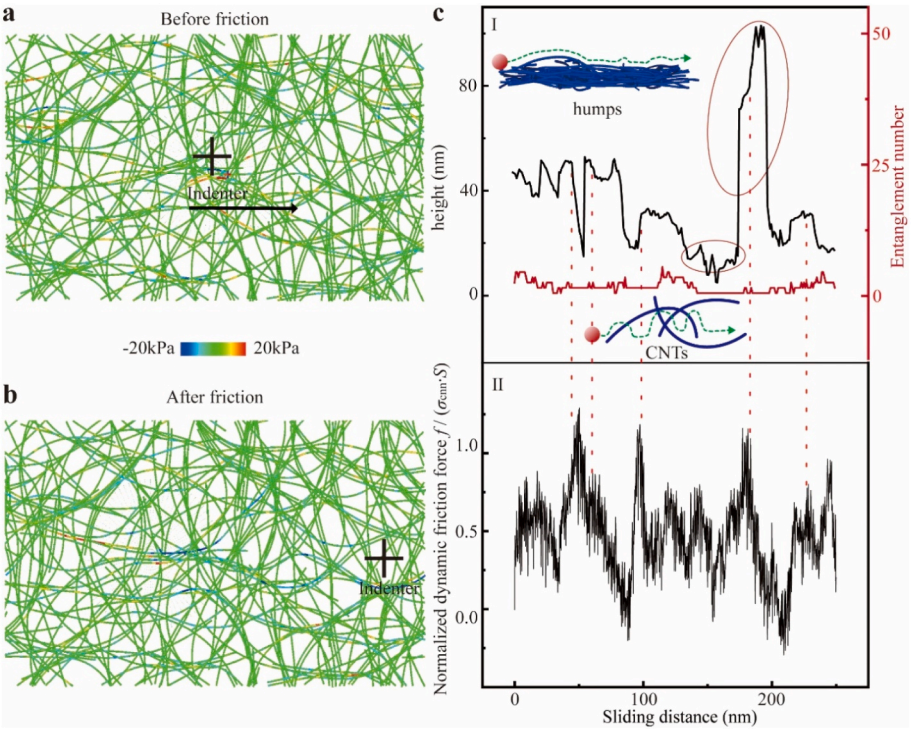

Fig. 3. The friction behavior of an indenter in a "supported" state. (a-b) Top view of CNNs color-coded by the value of σ_{xx} before and after friction for an indenter marked by the black cross in the direction pointed by the black arrow; (c-I) The relative height of the region in the sliding direction and the entanglement number of the CNN film, and (c-II) the normalized dynamic friction force on the indenter at the sliding distance. Two insets in c-I schematically show the two kinds of roughness of CNN surface due to the hump of CNT assembly and the unevenness of a single CNT. The green dotted lines show the moving trajectory of the indenter. (A colour version of this figure can be viewed online.)

3.3. Friction behavior of an indenter in a "trapped" state

To study the friction behavior of an indenter in a "trapped" state, we randomly choose a combination of the two factors of $R = 6.3$ and $\sigma = 13$ which corresponds to a point above the red boundary line in the σ-R plane and highlighted by the red circle in Fig. 2. Fig. 4a shows the top view of the topological structure color-coded by the corresponding stress component σ_{xx} of the CNN film at the initial state, an intermediate state and the final state, respectively. Fig. 4a–I shows the initial position of the indenter signed by a black cross in a "trapped" state on the CNN film. A cavity forms under the indenter after the press-in process and the high tensile/compressive stress states are triggered in the CNTs around the indenter due to relatively heavy squeeze. When the indenter slides, the CNTs ahead of the indenter would be further squeezed and gathered, which leads to a larger stress concentration in a wider range as shown in Fig. 4a–II. We observe an interesting corrugated stripe (highlighted by the black lines in Fig. 4a–III) formed by heavily bended CNTs behind the indenter as it slides away. What's special, high tensile/compressive stress states emerge not only in the CNTs near the sliding path of the indenter, but also at a distance far from the indenter, showing a nonlocal characteristic. At the same time, the network structure obviously reconstructs accompanying with plastic deformation and bond-breaking in the CNNs. The similar phenomenon of the scratching/gathering of CNTs under friction has also been observed in the experiment by Zhou et al. [58] as shown in Fig. 4b. Fig. 4b–I shows the initial state of the CNTs well-arranged along the direction pointed by the white line. Then, an indenter slides in the direction pointed by the red arrow and induces the CNTs bending towards the moving direction of the indenter, forming the similar corrugated stripe as shown in Fig. 4b–II. To be noticed, due to the large reconstruction of microstructures of CNNs, the dynamic friction force of the indenter in the "trapped" state is much larger than that in the case of "supported" state, as shown in Fig. 4c. Besides of those friction source mentioned in the "supported" state, the nonlocal corrugated stripes with larger unevenness and broken bonds of CNTs in the "trapped" state also contribute to the friction resistance to the indenter. In addition, in contrast to the almost unchanged entanglement number in the "supported" state as shown in Fig. 3c–I, the entanglement number increases constantly with the increased friction distance as the blue solid line shown in Fig. 4c because of the drastic nonlocal reconstruction of the CNN structure as shown in Fig. 4a–II and 4a-III.

3.4. The effect of normal pressure

As discussed in Fig. 2, the normal pressure is one of the two key factors responsible for the initial "supported" or "trapped" state of an indenter. We further study the effect of normal pressure on friction behaviors for the two initial states as shown in Fig. 5. We find that if the normal pressure is less than a critical stress σ_c for a given indenter, as shown on the left side of the dotted line, the indenter is in the "supported" state and the corresponding average friction force (the black line) is nearly independent on normal pressure. Thus, according to the

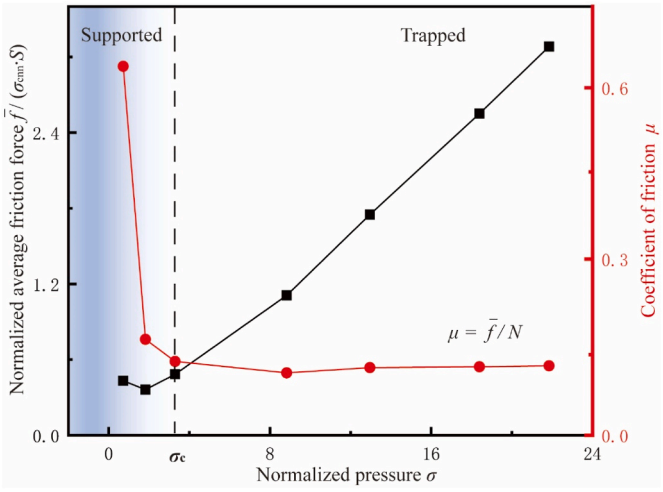

Fig. 5. Normalized average friction force $\bar{f}/(\sigma_{cnn}\cdot S)$ (obtained by averaging the dynamic friction force of the indenter) and corresponding COFμ as a function of normal pressure. (A colour version of this figure can be viewed online.)

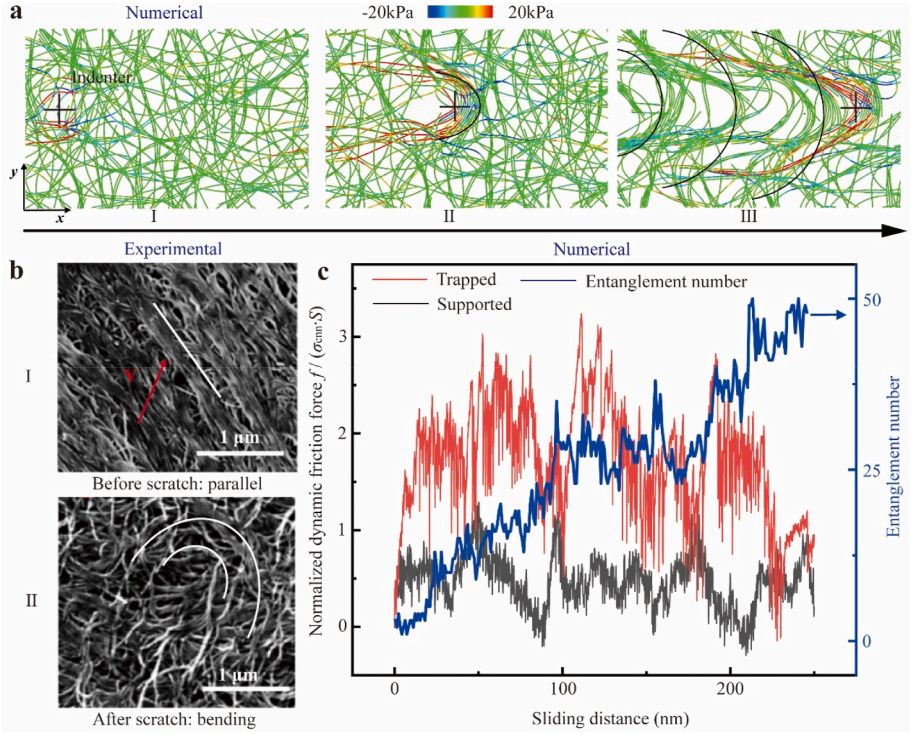

Fig. 4. The friction behavior of an indenter in a "trapped" state. (a-I,II,III) The top view of the microstructural evolution of the CNN film in friction process color-coded by the stress σ_{xx} (tension parts are in red and compression parts are in blue). The position of the indenter is marked by a black cross. Black curves show the corrugated structure formed by CNTs. (b-I,II) The scratching of CNTs on the surface of CNNs in the experimental literature [58], the white lines show the initial orientation of CNTs and bending after friction of an indenter, respectively; the red arrow shows the sliding direction. (c) The comparison of normalized dynamic friction force for the indenter initially in a "trapped" (red) state with that in a "supported" (black) one; the entanglement number as a function of the sliding distance. (A colour version of this figure can be viewed online.)

formula $\mu = \bar{f}/N$, the corresponding COF (the red line) is decreased greatly as an increased normal pressure as given in Fig. 5. If a larger normal pressure is adopted, the indenter would be in a "trapped" state and the average friction force becomes linearly dependent on normal pressure as shown on the right side of the dotted line, which is qualitatively consistent with the experimental observation by Babu et al. [59], who performed scratch testing on MWCNT/Aluminum fiber reinforced polymers by using a nano-sized indenter. Therefore, the COF is nearly invariant with an increased normal pressure. According to the discussion in Fig. 3, the friction force of an indenter in a "supported" state is mainly induced by local elastic contact between the indenter and CNTs. Due to the porous topology of CNNs, the effective contact area between CNTs and the indenter has no obvious increase if a smaller normal pressure is adopted, which is responsible for the almost unchanged friction force. The similar phenomenon has also been reported in the experiments [43,60]. However, for the "trapped" state of the indenter, the press-in depth would increase as an increased normal pressure, as a result, more CNTs would be scratched in the following friction process as discussed in Fig. 4, which induces larger friction resistance.

3.5. The effect of sliding velocity of an indenter

Fig. 6a shows the normalized average friction force $\bar{f}/(\sigma_{cnn} \cdot S)$ as a function of the sliding speed of an indenter initially in a "supported" or "trapped" state. If the indenter is in a "supported" state, the average friction force increases linearly with an increased sliding velocity of the indenter, reflecting a linearly viscoelastic property of CNN film materials. If the indenter is in a "trapped" state, the average friction force increases nonlinearly. In this case, there exists a critical sliding velocity v_c, the average friction force is independent on the sliding velocity if $v \leq v_c$ and then it increases nonlinearly as $v > v_c$. Fig. 6b shows the topological structures of the CNN film after friction of the indenter in the "supported" state at a speed of 100 m/s, no CNT breaks in this case as the red beads shown in Fig. 6b. However, if the indenter is initially in a "trapped" state and slides at the same speed, CNTs have no enough time to relax and would break as the red broken CNTs shown in Fig. 6c, which is responsible for the nonlinear friction behavior of the indenter.

3.6. The effect of crosslink density

Furthermore, we study the effect of the crosslink density of CNNs on the friction behavior of an indenter at a given normalized pressure of $\sigma = 13$ and the sliding velocity of $v = 10$ m/s. Here, the crosslink density is defined as the average number of crosslinks on each CNT. Nine sets of crosslink density from 1% to 92% are selected for systematic simulations. Fig. 7a shows that there exists a critical crosslink density $\rho_c \sim 22\%$ as signified by the dashed line, as $\rho < \rho_c$, the indenter is initially in a "trapped" state and the COF is nearly independent on the crosslink density; as $\rho > \rho_c$, the CNNs is highly interconnected and strengthened by more crosslinks, the initial state of the indenter would change to the "supported" state under the same normalized pressure. In this case, the COF is almost linearly decreased with an increased crosslink density. Fig. 7b and c shows the topological structures of the CNNs with the smaller and larger crosslink density after friction process. As shown in Fig. 7b, because the indenter is in the "trapped" state, the resulting CNN structure is similar to that in Fig. 4, i.e., the obvious corrugated stripes emerge along the sliding path of the indenter as indicated by the black dotted line. In contrast, as shown in Fig. 7c, the network structure of CNNs with larger crosslink density remains intact as that in Fig. 3, because the indenter is in the "supported" state.

For CNNs with a low crosslink density $\rho < \rho_c$, it is easier for the indenter to be pressed into the CNNs to be a "trapped" state. And the loose structure of the CNNs could not be strengthened completely as long as $\rho < \rho_c$, which is responsible for the unchanged COF with an increased ρ. As $\rho > \rho_c$, the CNNs is strongly interconnected to be a higher integrity and becomes smoother as more crosslinks are included. As a result, both the plastic deformation and bond breaking which are the source of friction resistance, are reduced accordingly. Thus, a reduced coefficient of friction can be obtained as an increased ρ. This finding is qualitatively consistent with the experimental result obtained by Kamal Yusoh [61] who studied the effect of concentration of CNTs on the scratch properties of polyurethane nanocomposites, and found that the scratch depth can be dramatically reduced with only 1 wt% single-walled CNTs included as crosslinkers.

4. Conclusions

In this paper, we systematically study the friction behavior of CNNs by using CGMD simulations. First, two initial contacting states of the indenter, "supported" and "trapped", are found by pressing the indenter into the surface, giving a new perspective for studying friction properties of porous material. Second, for a given normalized size, friction deformation behavior of CNNs highly depends on the initial contacting state. The "supported" state indicates a slight contact triggered by the "local

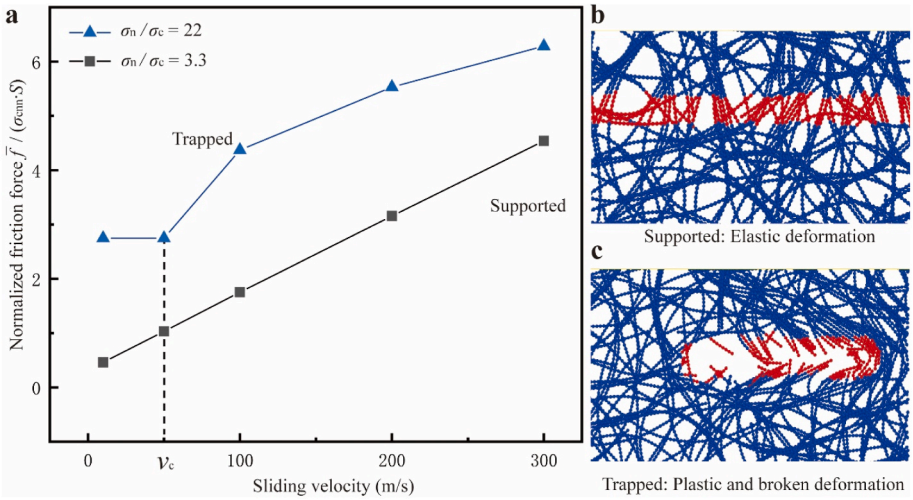

Fig. 6. The effect of the sliding velocity of an indenter on friction behaviors. (a) Normalized average friction force $\bar{f}/(\sigma_{cnn} \cdot S)$ as a function of the sliding velocity of an indenter in the two states; (b, c) The top view of CNNs with the touched CNT beads (marked in red) by the indenter in the "supported" state with σ = 3.3 and the "trapped" state with σ = 22 at the same sliding velocity of 100 m/s. (A colour version of this figure can be viewed online.)

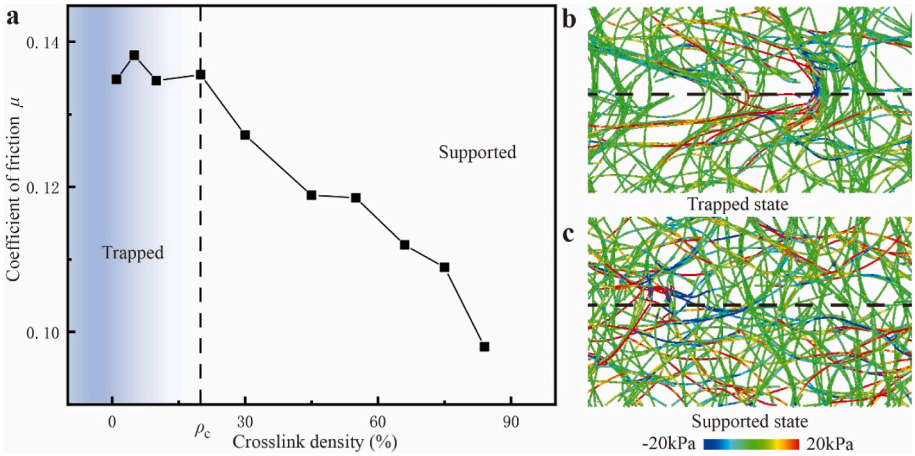

Fig. 7. The effect of crosslink density of CNNs on the friction behavior of an indenter. (a) The coefficient of friction as a function of crosslink density; (b, c) The top view of the topological structures of CNNs with a low and a high crosslink density. The black dotted lines show the sliding trajectory of the indenter. (A colour version of this figure can be viewed online.)

elastic contact" of surrounding CNTs and shows an elastic and temporary deformation. However, the "trapped" state means a heavy contact caused by nonlocal plastic accumulation of large-scope affected and rearranged CNTs. Third, the friction response to the normal pressure, sliding velocity and crosslink density are further studied: (1) A critical normalized pressure σ_c divides the two contacting states of the indenter for a given normalized indenter size R. In the "supported" state ($\sigma < \sigma_c$), the indenter slightly contacts with the film, resulting a steady friction force and a decreased COF. However, as the normal pressure increases, most part of the indenter would be immersed in the film to be the "trapped" state ($\sigma > \sigma_c$), which leads to a linearly increased friction force; (2) In a "supported" state, the elastic deformation of CNTs is responsible for the linearly increased friction force with the sliding velocity, whereas in the "trapped" state, plasticity and bond breaking would cause a nonlinearly increased normalized friction force when the critical velocity v_c is exceeded; (3) Cross-linking greatly strengthens the interconnection between CNTs and can further tune the initial contact state of an indenter at a given normalized size R and pressure σ. The CNNs with low crosslink density ($\rho < \rho_c$) have an unchanged COF due to its loose structure, while the CNNs with high crosslink density ($\rho > \rho_c$) have a decreased COF with an increased crosslink density due to the improved integrity of CNN structures.

These results pave the way for understanding the friction between CNNs and CNN-based composites with a real rough surface having many humps and of great significance for optimization design of the related composite materials.

CRediT authorship contribution statement

Tianxiong Hu: Conceptualization, Methodology, Software, Formal analysis, Investigation, Data curation, Writing – original draft, Writing – review & editing, Visualization. **Guian Qian:** Resources, Writing – review & editing. **Xianqian Wu:** Resources, Writing – review & editing, Validation. **Chao Wang:** Funding acquisition, Resources, Software, Supervision, Writing – review & editing, Project administration.

Declaration of competing interest

The authors declare that they have no known competing financial interests or personal relationships that could have appeared to influence the work reported in this paper.

Acknowledgments

C.W. acknowledges the support of NSFC through Grants #11972348, #11790292, Strategic Priority Research Program of the Chinese Academy of Sciences (Grant No. XDB22040503).

Appendix A. Supplementary data

Supplementary data to this article can be found online at https://doi.org/10.1016/j.carbon.2022.08.042.

References

[1] D. Li, X. Zhou, X. Guo, B. Yuan, Y. Liu, C.M. Ortega, L. Sun, Z. Liu, A novel Fe_3O_4/buckypaper composite as free-standing anode for lithium-ion battery, J. Alloys Compd. 657 (2016) 109–114.
[2] M.F. Yu, O. Lourie, M.J. Dyer, K. Moloni, T.F. Kelly, R.S. Ruoff, Strength and breaking mechanism of multiwalled carbon nanotubes under tensile load, Science 287 (5453) (2000) 637–640.
[3] H. Koerner, G. Price, N.A. Pearce, M. Alexander, R.A. Vaia, Remotely actuated polymer nanocomposites - stress-recovery of carbon-nanotube-filled thermoplastic elastomers, Nat. Mater. 3 (2) (2004) 115–120.
[4] E.W. Keefer, B.R. Botterman, M.I. Romero, A.F. Rossi, G.W. Gross, Carbon nanotube coating improves neuronal recordings, Nat. Nanotechnol. 3 (7) (2008) 434–439.
[5] R. Yadav, M. Tirumali, X.G. Wang, M. Naebe, B. Kandasubramanian, Polymer composite for antistatic application in aerospace, Def Technol. 16 (1) (2020) 107–118.
[6] J. Choi, J.I. Lee, Y. Eun, M.O. Kim, J. Kim, Aligned carbon nanotube arrays for degradation-resistant, intimate contact in micromechanical devices, Adv. Mater. 23 (19) (2011) 2231–+.
[7] R. Das, S.B.A. Hamid, M.E. Ali, A.F. Ismail, M.S.M. Annuar, S. Ramakrishna, Multifunctional carbon nanotubes in water treatment: the present, past and future, Desalination 354 (2014) 160–179.
[8] L.M. Peng, Z.Y. Zhang, S. Wang, Carbon nanotube electronics: recent advances, Mater. Today 17 (9) (2014) 433–442.
[9] W.J. Ma, L. Song, R. Yang, T.H. Zhang, Y.C. Zhao, L.F. Sun, Y. Ren, D.F. Liu, L. F. Liu, J. Shen, Z.X. Zhang, Y.J. Xiang, W.Y. Zhou, S.S. Xie, Directly synthesized strong, highly conducting, transparent single-walled carbon nanotube films, Nano Lett. 7 (8) (2007) 2307–2311.
[10] Y. Li, M. Kroger, A theoretical evaluation of the effects of carbon nanotube entanglement and bundling on the structural and mechanical properties of buckypaper, Carbon 50 (5) (2012) 1793–1806.
[11] I.W.P. Chen, R. Liang, H.B. Zhao, B. Wang, C. Zhang, Highly conductive carbon nanotube buckypapers with improved doping stability via conjugational cross-linking, Nanotechnology 22 (48) (2011), 485708.
[12] M.B. Jakubinek, B. Ashrafi, J.W. Guan, M.B. Johnson, M.A. White, B. Simard, 3D chemically cross-linked single-walled carbon nanotube buckypapers, RSC Adv. 4 (101) (2014) 57564–57573.
[13] C. Wang, E.L. Gao, L.F. Wang, Z.P. Xu, Mechanics of network materials with responsive crosslinks, C R Mec 342 (5) (2014) 264–272.
[14] T. Yang, C. Wang, Z.B. Wu, Crosslink-tuned large-deformation behavior and fracture mode in buckypapers, Carbon 159 (2020) 412–421.

[15] B. Xie, Y.L. Liu, Y.T. Ding, Q.S. Zheng, Z.P. Xu, Mechanics of carbon nanotube networks: microstructural evolution and optimal design, Soft Matter 7 (21) (2011) 10039–10047.
[16] S.J. Wang, J.H. Lin, Z. Xu, Z.P. Xu, Understanding macroscopic assemblies of carbon nanostructures with microstructural complexity, Composites Part A 143 (2021), 106318.
[17] Y. Wu, C. Wang, T. Yang, Aggregation of nanoparticles and their effect on mechanical properties of carbon nanotube networks, Comput. Mater. Sci. 202 (2022), 110970.
[18] C. Wang, L.F. Wang, Z.P. Xu, Enhanced mechanical properties of carbon nanotube networks by mobile and discrete binders, Carbon 64 (2013) 237–244.
[19] S.J. Wang, E.L. Gao, Z.P. Xu, Interfacial failure boosts mechanical energy dissipation in carbon nanotube films under ballistic impact, Carbon 146 (2019) 139–146.
[20] K.L. Xiao, X.D. Lei, Y.Y. Chen, Q. An, D.M. Hu, C. Wang, X.Q. Wu, C.G. Huang, Extraordinary impact resistance of carbon nanotube film with crosslinks under micro-ballistic impact, Carbon 175 (2021) 478–489.
[21] J.G. Yu, C.X. Zhai, M.C. Wang, Z.L. Cai, J.J. Yeo, Q.X. Zhang, C.Y. Zhao, S.C. Lin, Hybridly double-crosslinked carbon nanotube networks with combined strength and toughness via cooperative energy dissipation, Nanoscale 14 (6) (2022) 2434–2445.
[22] M. Xu, D.N. Futaba, T. Yamada, M. Yumura, K. Hata, Carbon nanotubes with temperature-invariant viscoelasticity from -196 °C to 1000 °C, Science 330 (6009) (2010) 1364–1368.
[23] Y. Li, M. Kroger, Viscoelasticity of carbon nanotube buckypaper: zipping-unzipping mechanism and entanglement effects, Soft Matter 8 (30) (2012) 7822–7830.
[24] X.D. Yang, P.F. He, H.J. Gao, Modeling frequency- and temperature-invariant dissipative behaviors of randomly entangled carbon nanotube networks under cyclic loading, Nano Res. 4 (12) (2011) 1191–1198.
[25] F.J. Xu, B.C. Wei, W. Liu, H.F. Zhu, Y.Y. Zhang, Y.P. Qiu, In-plane mechanical properties of carbon nanotube films fabricated by floating catalyst chemical vapor decomposition, J. Mater. Sci. 50 (24) (2015) 8166–8174.
[26] Y.J. Ma, X.F. Yao, Q.S. Zheng, Y.J. Yin, D.J. Jiang, G.H. Xu, F. Wei, Q. Zhang, Carbon nanotube films change Poisson's ratios from negative to positive, Appl. Phys. Lett. 97 (6) (2010), 061909.
[27] A. Rawal, D. Singh, A. Rastogi, S. Sharma, On the origin of negative Poisson's ratio in buckypapers, Extreme Mech. Lett. 42 (2021), 101059.
[28] F. Pan, Y.L. Chen, Q.H. Qin, Stiffness thresholds of buckypapers under arbitrary loads, Mech. Mater. 96 (2016) 151–168.
[29] Y.L. Chen, F. Pan, Z.Y. Guo, B. Liu, J.Y. Zhang, Stiffness threshold of randomly distributed carbon nanotube networks, J. Mech. Phys. Solid. 84 (2015) 395–423.
[30] F. Deng, M. Ito, T. Noguchi, L.F. Wang, H. Ueki, K. Niihara, Y.A. Kim, M. Endo, Q. S. Zheng, Elucidation of the reinforcing mechanism in carbon nanotube/rubber nanocomposites, ACS Nano 5 (5) (2011) 3858–3866.
[31] M. Wang, N. Li, G.D. Wang, W.L. Shao, D.Z. Qi, L.L. Xi, High-sensitive flexural sensors for health monitoring of composite materials using embedded carbon nanotube (CNT) buckypaper, Compos. Struct. 261 (2021), 113280.
[32] A. Mehmood, N.M. Mubarak, M. Khalid, P. Jagadish, R. Walvekar, E.C. Abdullah, Graphene/PVA buckypaper for strain sensing application, Sci Rep-Uk 10 (1) (2020) 20106.
[33] M.Y. Fard, Carbon nanotube network and interphase in buckypaper nanocomposites using atomic force microscopy, Int. J. Mech. Sci. 212 (2021), 106811.
[34] M. Ito, T. Noguchi, H. Ueki, K. Takeuchi, M. Endo, Carbon nanotube enables quantum leap in oil recovery, Mater. Res. Bull. 46 (9) (2011) 1480–1484.
[35] X. Wang, Z.Z. Yong, Q.W. Li, P.D. Bradford, W. Liu, D.S. Tucker, W. Cai, H. Wang, F.G. Yuan, Y.T. Zhu, Ultrastrong, stiff and multifunctional carbon nanotube composites, Mater Res. Lett. 1 (1) (2013) 19–25.
[36] B. Ashrafi, J.W. Guan, V. Mirjalili, P. Hubert, B. Simard, A. Johnston, Correlation between Young's modulus and impregnation quality of epoxy-impregnated SWCNT buckypaper, Composites Part A 41 (9) (2010) 1184–1191.
[37] L.Y. Lin, X.Q. Wang, B. Yang, L. Zhang, Z.P. Zhao, X.Q. Qu, Y. Lu, X.W. Jiang, S. W. Lu, Condition monitoring of composite over wrap pressure vessels based on buckypaper sensor and MXene sensor, Compos. Commun. 25 (2021), 100699.
[38] J. Umeda, B. Fugetsu, E. Nishida, H. Miyaji, K. Kondoh, Friction behavior of network-structured CNT coating on pure titanium plate, Appl. Surf. Sci. 357 (2015) 721–727.
[39] J.Q. Hu, X.M. Liu, Y.G. Wei, Effect of plasticity and adhesion on the stick-slip transition at nanoscale friction, Tribol. Int. 164 (2021), 107230.
[40] M. Urbakh, J. Klafter, D. Gourdon, J. Israelachvili, The nonlinear nature of friction, Nature 430 (6999) (2004) 525–528.
[41] B.L. Pan, S.P. Zhang, W.Z. Li, J. Zhao, J.L. Liu, Y.Q. Zhang, Y.Z. Zhang, Tribological and mechanical investigation of MC nylon reinforced by modified graphene oxide, Wear 294 (2012) 395–401.
[42] M. Kalin, M. Zalaznik, S. Novak, Wear and friction behaviour of poly-ether-ether-ketone (PEEK) filled with graphene, WS_2 and CNT nanoparticles, Wear 332 (2015) 855–862.
[43] J. Fei, H.J. Li, Y.W. Fu, L.H. Qi, Y.L. Zhang, Effect of phenolic resin content on performance of carbon fiber reinforced paper-based friction material, Wear 269 (7–8) (2010) 534–540.
[44] R. Nandan, T. DebRoy, H.K.D.H. Bhadeshia, Recent advances in friction-stir welding - process, weldment structure and properties, Prog. Mater. Sci. 53 (6) (2008) 980–1023.
[45] P.H. Cornuault, L. Carpentier, Tribological mechanisms involved in friction wood welding, Tribol. Int. 141 (2020), 105963.
[46] S. Cranford, H.M. Yao, C. Ortiz, M.J. Buehler, A single degree of freedom 'lollipop' model for carbon nanotube bundle formation, J. Mech. Phys. Solid. 58 (3) (2010) 409–427.
[47] S. Cranford, M.J. Buehler, In silico assembly and nanomechanical characterization of carbon nanotube buckypaper, Nanotechnology 21 (26) (2010), 265706.
[48] J. Ji, J. Zhao, W. Guo, Novel nonlinear coarse-grained potentials of carbon nanotubes, J. Mech. Phys. Solid. 128 (2019) 79–104.
[49] W.F. Van Gunsteren, H.J. Berendsen, Molecular dynamics: perspective for complex systems, Biochem. Soc. Trans. 10 (5) (1982) 301–305.
[50] J.N. Coleman, W.J. Blau, A.B. Dalton, E. Munoz, S. Collins, B.G. Kim, J. Razal, M. Selvidge, G. Vieiro, R.H. Baughman, Improving the mechanical properties of single-walled carbon nanotube sheets by intercalation of polymeric adhesives, Appl. Phys. Lett. 82 (11) (2003) 1682–1684.
[51] P. Liu, Y.F. Tan, D.C.M. Hu, D. Jewell, H.M. Duong, Multi-property enhancement of aligned carbon nanotube thin films from floating catalyst method, Mater. Des. 108 (2016) 754–760.
[52] S. Sakurai, F. Kamada, D.N. Futaba, M. Yumura, K. Hata, Influence of lengths of millimeter-scale single-walled carbon nanotube on electrical and mechanical properties of buckypaper, Nanoscale Res. Lett. 8 (2013) 546.
[53] C. Wang, S.H. Chen, Viscoelastic properties of randomly entangled carbon nanotube networks under cyclic tension loading, Comput. Mater. Sci. 119 (2016) 46–51.
[54] C. Wang, B. Xie, Y.L. Liu, Z.P. Xu, Mechanotunable microstructures of carbon nanotube networks, ACS Macro Lett. 1 (10) (2012) 1176–1179.
[55] S. Plimpton, Fast parallel algorithms for short–range molecular dynamics, J. Comput. Phys. 117 (1995) 1–19.
[56] A. Stukowski, Visualization and analysis of atomistic simulation data with OVITO-the open visualization tool modelling, Model. Simulat. Mater. Sci. Eng. 18 (2010), 015012.
[57] Y. Tsukiyama, N. Umehara, M. Kusunoki, Nanowear characteristics of carbon nanotube film made by surface decomposition of SiC, J. Adv. Mech. Des. Syst. 4 (1) (2010) 373–382.
[58] M. Zhou, K. Liu, J. Wan, X. Li, K.L. Jiang, H.B. Zeng, X.J. Zhang, Y.G. Meng, S. Z. Wen, H.W. Zhu, Y. Tian, Anisotropic interfacial friction of inclined multiwall carbon nanotube array surface, Carbon 50 (15) (2012) 5372–5379.
[59] J.S.S. Babu, A. Srinivasan, C.G. Kang, Tribological and nano-scratch properties of aluminum (A356) based hybrid composites reinforced with MWCNTs/alumina fiber, Met. Mater. Int. 27 (9) (2021) 3666–3680.
[60] P. Gopal, L.R. Dharani, F.D. Blum, Load, speed and temperature sensitivities of a carbon-fiber-reinforced phenolic friction material, Wear 181 (1995) 913–921.
[61] K.B. Yusoh, Scratch property of polyurethane nanocomposites studied by nanoindentation, J. Appl. Sci. Eng. (2015) 1819–6608.